High-Transmission Ultrathin Huygens' Metasurface with 360° Phase Control by Using Double-Layer Transmitarray Elements

Liang Wei Wu, Hui Feng Ma,* Yue Gou, Rui Yuan Wu, Zheng Xing Wang, Meng Wang, Xinxin Gao, and Tie Jun Cui†

State Key Laboratory of Millimeter Waves, School of Information Science and Engineering, Southeast University, Nanjing 210096, China

(Received 24 March 2019; revised manuscript received 28 May 2019; published 7 August 2019)

Metasurfaces, which are planar surfaces or interfaces constructed by placing subwavelength scatterers into a two-dimensional array pattern, have attracted much attention in recent years. However, it has been shown that transmission-type metasurfaces without vias are hard to simultaneously achieve high transmission and 360° phase control when the number of cascaded layers is less than three. An ultrathin Huygens' metasurface composed of only double-layer transmitarray elements without vias is proposed to achieve both high transmission (−2.5-dB criteria) and 360° phase control. Benefiting from the antisymmetric design of the double-layer transmitarray element, the proposed Huygens' metasurface excites both electric and magnetic dipole resonances with mutual interference, allowing the realization of high transmission and 360° phase control at the same time, which cannot be fulfilled by symmetric unit structures. Based on the ultrathin Huygens' metasurface, a high-gain transmitarray antenna is designed, fabricated, and measured, which can achieve high aperture efficiency up to 61.04% with a very small thickness of only 0.033 wavelengths at a microwave frequency of 13 GHz.

DOI: 10.1103/PhysRevApplied.12.024012

I. INTRODUCTION

Metamaterials are composed of artificial subwavelength unit structures with periodic or aperiodic arrangement, having the ability to flexibly manipulate electromagnetic (em) waves [1–3]. Based on metamaterials, many fantastic works have been presented, such as negative refraction [4], invisibility cloaking [5,6], transformation-optics lenses [7], and so on [8]. Metasurfaces can be treated as planar metamaterials by placing the subwavelength scatterers into a two-dimensional (2D) pattern on a surface, which also has powerful abilities in the manipulation of em waves [9–24]. Metasurfaces are usually classified into two types in reflection and transmission modes. For the reflection-type metasurface, it is easy to simultaneously achieve high reflection and 360° phase control by using a single-layer reflectarray [12]. For the transmission-type metasurface, however, it is difficult to simultaneously achieve high transmission and 360° phase control by using a single- or double-layer transmitarray [12,21,23].

The transmitarray, composed of multilayer frequency selective surfaces (M FSSs), can be regarded as a kind of transmission-type metasurface. Many efforts have been made to achieve high transmission and full 360° phase control at the same time with multilayer transmitarrays [16,18,21], but the number of layers cannot be effectively reduced. In Ref. [21], it was proved that the transmission phase of M FSSs has a limit, that is, the full 360° phase control of a transmitarray with −3-dB transmission criterion requires at least three layers of FSSs. In order to further improve the phase range of the transmitarray, vertical vias have been employed in double-layer FSS structures to augment the transmission magnitude [23]. However, this effort can only achieve a maximum 305° transmission phase shift. Each layer of the M FSSs is usually assumed to have identical patterns of electric dipole resonances, so the multilayer structures are required to obtain a large transmission phase range.

Huygens' surfaces are composed of both spatially varying electric and magnetic dipole resonances, which can be used to manipulate the em waves arbitrarily passing through the surfaces [24]. Metasurfaces designed with the theory of Huygens' surfaces, which are also called Huygens' metasurfaces, have been widely studied recently [25–35]. A cavity excited Huygens' metasurface antenna has been presented in Ref. [34], which displays significant advantages of near-unity aperture illumination efficiency, low side-lobe level (SLL), and high realized gain. In addition, the Huygens' metasurface can also be used to design leaky wave antennas [30] and beam focusing [35]. Generally, there are two ways to construct the elements of Huygens' metasurfaces: wire-loop volume unit structures [24,26,31] and multilayer cascaded surface unit structures

*hfma@seu.edu.cn
†tjcui@seu.edu.cn

[27,29]. Most of the Huygens' metasurfaces are designed based on multilayer cascaded conducting surfaces whose thicknesses are dependent on the number of layers. The fewer the layer number is, the thinner the thickness is.

To the best of our knowledge, no work has been presented to simultaneously realize high transmission and full 360° phase control by using the transmission-type metasurfaces without vias with less than three layers. It was reported that full 360° phase control of cross-polarized waves by using only a single-layer metasurface was achieved, but all transmission efficiencies were lower than 50% [9,12,36]. Here, a Huygens' metasurface composed of double-layer transmitarray elements without vias is proposed to simultaneously achieve high transmission and a full 360° phase control in which the two layers of the unit cell contain a separate split ring (SR) and a rectangular metallic stub and the two SRs on different layers are antisymmetrical. The thickness of the proposed Huygens' metasurface is 0.762 mm, which is only 0.033λ at the working frequency of 13 GHz. Because of the antisymmetry of SRs, the reverse currents on the arms of SRs are generated to introduce the magnetic dipole resonance, and the rectangular metallic stubs are placed inside SRs on each layer to introduce the electric dipole resonance. Hence, the ultrathin Huygens' metasurface with both electric and magnetic dipole resonances is constructed and high transmission with full 360° phase control can be simultaneously achieved, breaking the limitation of three layers by using traditional symmetric unit structures. Based on the proposed two-layer Huygens' metasurface, a high-gain ultrathin transmitarray antenna is designed, fabricated, and measured. The experimental results show that the aperture efficiency of the antenna can reach up to 61.04% at 13 GHz by using a corrugated horn as a feeding source. In addition, it is worth mentioning that the proposed double-layer unit structure has no vertical vias, and hence it can be easily extended to terahertz frequencies.

II. UNIT STRUCTURE AND THEORETICAL ANALYSIS

Figure 1 shows a typical sketch of a Huygens' surface under the illumination of normal incidence [27]. Assuming that the incident waves propagate normally from Region I to Region II by passing through the Huygens' surface, the wavefronts of the transmitted waves in Region II are totally tailored by manipulating the Huygens' metasurface. Based on microwave theory and equivalence principle, the normalized electric surface admittance ($Y_{ES}\eta_0$) and magnetic surface impedance (Z_{MS}/η_0) of the surface can be obtained from the transmission coefficients (T) and reflection coefficients (R) [27]

$$Y_{ES}\eta_0 = 2 \cdot \frac{1 - T - R}{1 + T + R}, \tag{1}$$

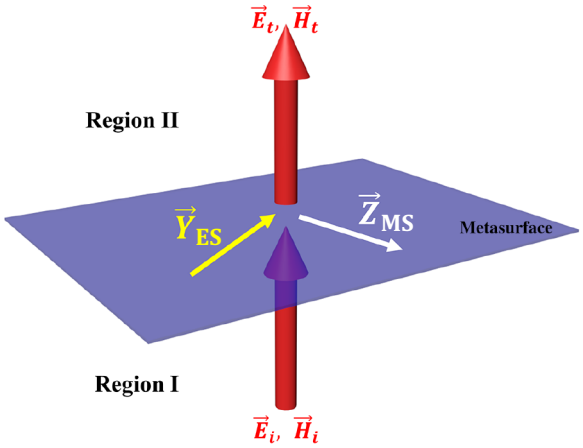

FIG. 1. A typical sketch of a Huygens' metasurface under the illumination of normal incidence.

$$Z_{MS}/\eta_0 = 2 \cdot \frac{1 - T + R}{1 + T - R}, \tag{2}$$

where η_0 is the wave impedance of free space. For a reflectionless Huygens' surface, the normalized electric surface admittance ($Y_{ES}\eta_0$) and magnetic surface impedance (Z_{MS}/η_0) must be equal [24].

Based on the above theory, a square double-layer metallic unit structure is proposed to construct the Huygens' metasurface with both electric and magnetic dipole resonances at the same time. The proposed unit structure contains two antisymmetric metallic SRs and metallic stubs spaced by a dielectric substrate of Roger's RO4350, as demonstrated in Fig. 2(a), which is called an antisymmetric

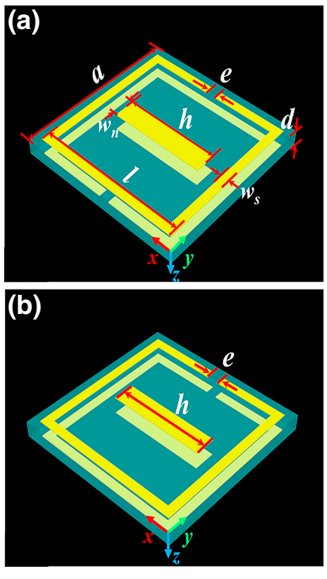

FIG. 2. The proposed double-layer antisymmetric unit structure and the traditional symmetric unit structure. (a) The antisymmetric unit structure. (b) The symmetric unit structure.

unit cell. The relative permittivity and loss tangent of Roger's RO4350 are $\epsilon_r = 3.48$ and $\tan\delta = 0.0037$, respectively, and the thickness of the substrate is $d = 0.762$ mm. The other parameters shown in Fig. 2(a) are $a = 8$ mm, $w_s = 0.4$ mm, $w_n = 1$ mm, $l = 7.2$ mm, and h and e are varied. For comparison, another double-layer symmetric unit structure is also studied, as shown in Fig. 2(b), which is almost the same as the antisymmetric unit structure except for the symmetric slotting of SRs.

Figure 3 demonstrates the transmission phases and amplitudes of both antisymmetric and symmetric unit structures that vary with e and h under the x polarized incident waves and distinctly different phase and amplitude responses for both unit structures are obtained. Figures 3(a) and 3(c) show the transmission phase and amplitude of the proposed antisymmetric unit cells, respectively, demonstrating that the full 360° phase control and high transmission can be simultaneously achieved. The region that can satisfy both full 360° phase control and high transmission is marked by a black dashed curve, as shown in both Figs. 3(a) and 3(c). However, for the symmetric unit cell, the maximum transmission phase range for a −3-dB transmission coefficient is only about 212° and it is marked by using a black dashed curve, as shown in Figs. 3(b) and 3(d), which is consistent with the conclusion presented in Ref. [21]: the limitation of the transmission phase range for a double-layer configuration is 228.5° (−3-dB criteria). Hence, the symmetric unit structures cannot be used for designing high-performance devices that require a 360° phase shift, even though they have a high transmission as shown in Fig. 3(d). We note that all the above full-wave simulations are performed by using the commercial software, CST Microwave Studio®, with a frequency domain solver.

In order to clearly show the essential difference between these two unit structures, the electric field and current distributions of the unit structures at 13 GHz are investigated, as illustrated in Fig. 4 with $e = 0.8$ mm and $h = 5.5$ mm. Figures 4(a) and 4(b) demonstrate the electric field amplitude distributions of the antisymmetric and symmetric unit structures, respectively, which imply that the strong electric response can be introduced by the LC resonances existing not only between the outer SRs and inner stubs, but also the SRs themselves. It should be noted that the effective inductances (L) come from the metallic conductors themselves, and the effective capacitances (C) come from the splits of SRs and the gaps between the outer SRs and inner stubs, respectively. Figures 4(c) and 4(e) demonstrate the current distributions of an antisymmetric unit cell on both the top and bottom layers, respectively, which show that the currents flow in the opposite direction along the horizontal arms (the x direction) of SRs on both sides. Hence, the electric dipoles introduced by the SRs on both sides have opposite phases in the x direction, which will be canceled by each other. Thus, the total electric dipole resonance is mainly contributed by the LC resonances between the outer SRs and inner stubs. In addition, because the current loops are formed along the horizontal arms of SRs on the top and bottom layers, the magnetic dipole resonances are introduced in the y direction. Hence,

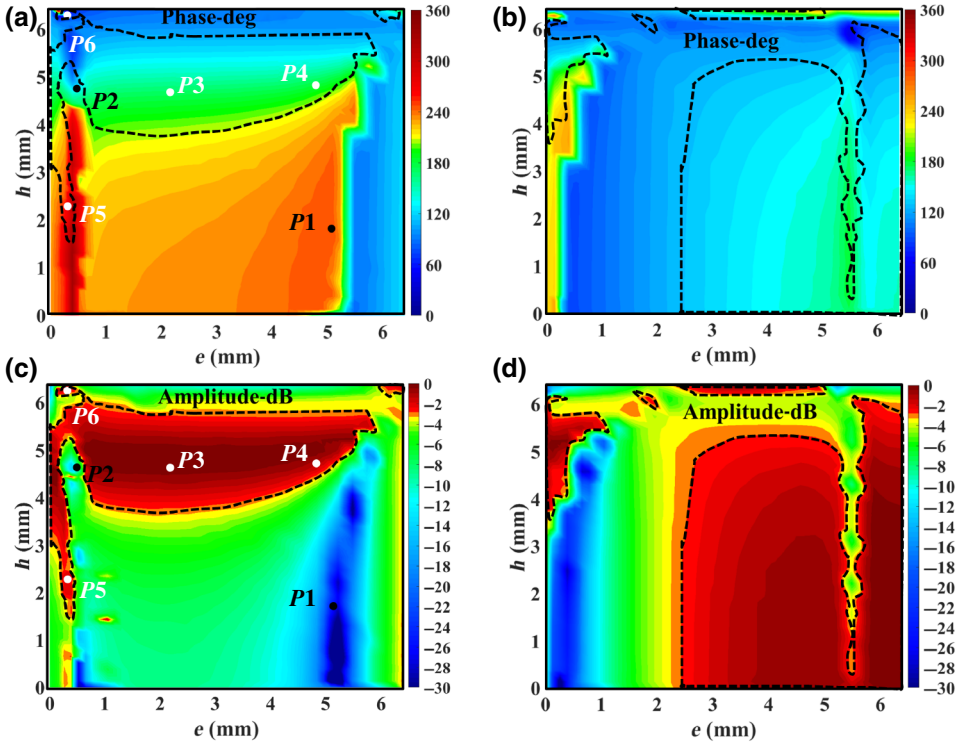

FIG. 3. The transmission phase and amplitude distributions of the proposed antisymmetric unit structure and traditional symmetric unit structure at 13 GHz varying with e and h. (a) The transmission phase distribution of the antisymmetric unit structure. (b) The transmission phase distribution of the symmetric unit structure. (c) The amplitude distribution of the antisymmetric unit structure. (d) The amplitude distribution of the symmetric unit structure.

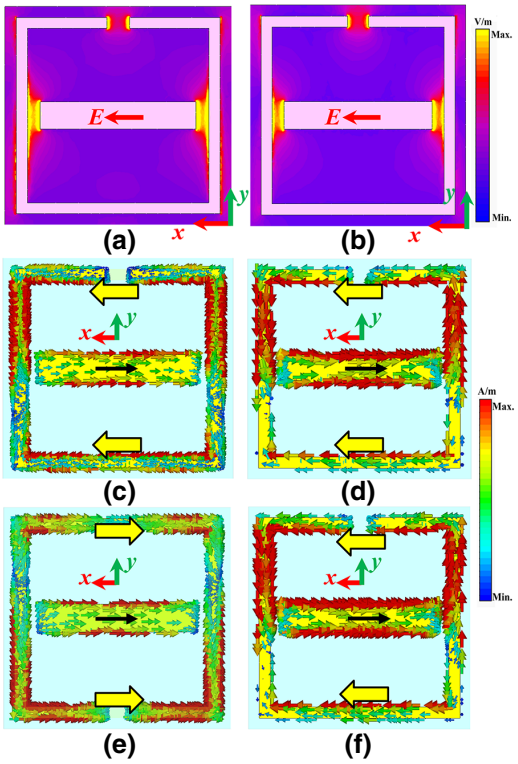

FIG. 4. The simulated electric field and current distributions of the proposed antisymmetric unit structure and traditional symmetric unit structure with $e = 0.8$ mm and $h = 5.5$ mm at 13 GHz. (a) The electric field distribution of the antisymmetric unit structure. (b) The electric field distribution of the symmetric unit structure. (c) The current distribution on the top layer of the antisymmetric unit structure. (d) The current distribution on the top layer of the symmetric unit structure. (e) The current distribution on the bottom layer of the antisymmetric unit structure (f) The current distribution on the bottom layer of the symmetric unit structure.

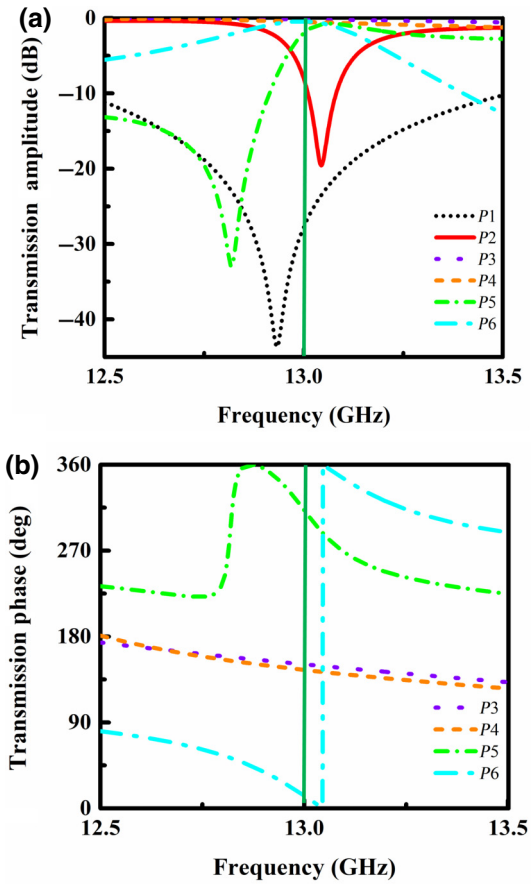

FIG. 5. The transmission amplitudes and phases of the proposed antisymmetric unit structures at points $P1$, $P2$, $P3$, $P4$, $P5$, and $P6$. (a) The transmission amplitudes of the unit cell at points $P1$, $P2$, $P3$, $P4$, $P5$, and $P6$. (b) The transmission phases of the unit cell at points $P3$, $P4$, $P5$, and $P6$.

the proposed double-layer antisymmetric unit structure can introduce both strong electric and magnetic dipole resonances, and high transmission and full 360° phase can be simultaneously achieved using the theory of Huygens' surface.

As to the symmetric unit structure, the currents flow in the same direction along the horizontal arms (the x direction) of SRs on both sides, as shown in Figs. 4(d) and 4(f). Hence, the electric dipoles introduced by the SRs have the same phases in the x direction, which will be enhanced by each other. Thus, the total electric dipole resonance is contributed by the LC resonances not only between the outer SRs and inner stubs, but also the SRs themselves. However, because the currents flow in the same direction along the horizontal arms of SRs on the top and bottom layers without a current loop formed, there is nearly no magnetic dipole resonance in the y direction, which is very different from the situation of the antisymmetric unit structures. Hence, the symmetric unit structure only has

TABLE I. The simulated surface impedances and/or admittances and transmission and/or reflection parameters of points $P1$, $P2$, $P5$, and $P6$ at 13 GHz.

Cell no.	Re ($Y_{ES}\eta$)	Re (Z_{ES}/η)	Im ($Y_{ES}\eta$)	Im (Z_{ES}/η)	Transmission Amplitude (dB)	Reflection Amplitude (dB)	Transmission Phase (°)
$P1$	0.0133	0.0080	0.3092	−17.6688	−27.70	−0.100	245.7
$P2$	0.0062	0.2375	−7.3302	−0.3302	−8.0198	−1.650	98.56
$P5$	0.3497	0.2887	1.2716	0.000	−2.000	−7.60	315.0
$P6$	0.0027	0.1070	−0.2358	−0.2261	−0.400	−25.72	13.50

TABLE II. The summarization of the unit structure that can cover 360° phase control with high transmission.

Transmission Phase (°)	Transmission Amplitude (dB)	Reflection Amplitude (dB)	e (mm)	h (mm)
0	−0.77	−11.7	0.22	6.4
32.2	−0.3	−22.4	0.13	6.3
62.7	−1.25	−8.13	0.3	6.3
89.8	−1.48	−7.3	0.5	5.9
120.2	−1.53	−6.8	1	5.5
149.9	−0.15	−15.3	1.5	5
179.5	−0.4	−10.8	2	4.5
210	−0.55	−10.37	0.2	4.1
239.6	−1.33	−7.53	0.28	3.3
268.3	−0.6	−19.6	0.35	3.3
302.4	−1.36	−11.09	0.38	2.35
328	−2.5	−6.51	0.39	0.7
359.5	−1.54	−8.07	0.18	6.38

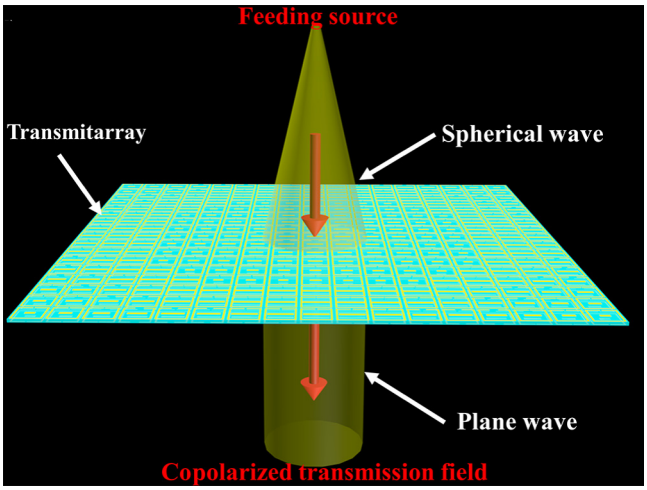

FIG. 6. The sketch of the transmitarray antenna.

electric dipole resonances, which satisfies the theory that the maximum transmission phase range is 228.5° for a double-layer transmitarray [21].

To further understand the characteristics of the antisymmetric unit structure, points $P1$, $P2$, $P3$, $P4$, $P5$, and $P6$ are sampled, as marked in Figs. 3(a) and 3(c), to investigate their transmission amplitudes and phases, which are illustrated in Fig. 5. As shown in Fig. 5(a), the transmission amplitudes are very low at points $P1$ and $P2$ due to the strong resonant peaks near the working frequency of 13 GHz, while the transmission amplitudes at points $P3$, $P4$, $P5$, and $P6$ are high. Since there is no resonance at points $P3$ and $P4$ around 13 GHz, the transmission phase curves are smooth, as shown in Fig. 5(b). Different from those of points $P3$ and $P4$, although the transmission efficiencies are high, points $P5$ and $P6$ have strong resonances near 13 GHz, and hence the transmission phase curves become steep at 13 GHz, and transmission phases with a large variation range can be achieved.

In addition, both the normalized electric surface admittance ($Y_{ES}\eta$) and magnetic surface impedance

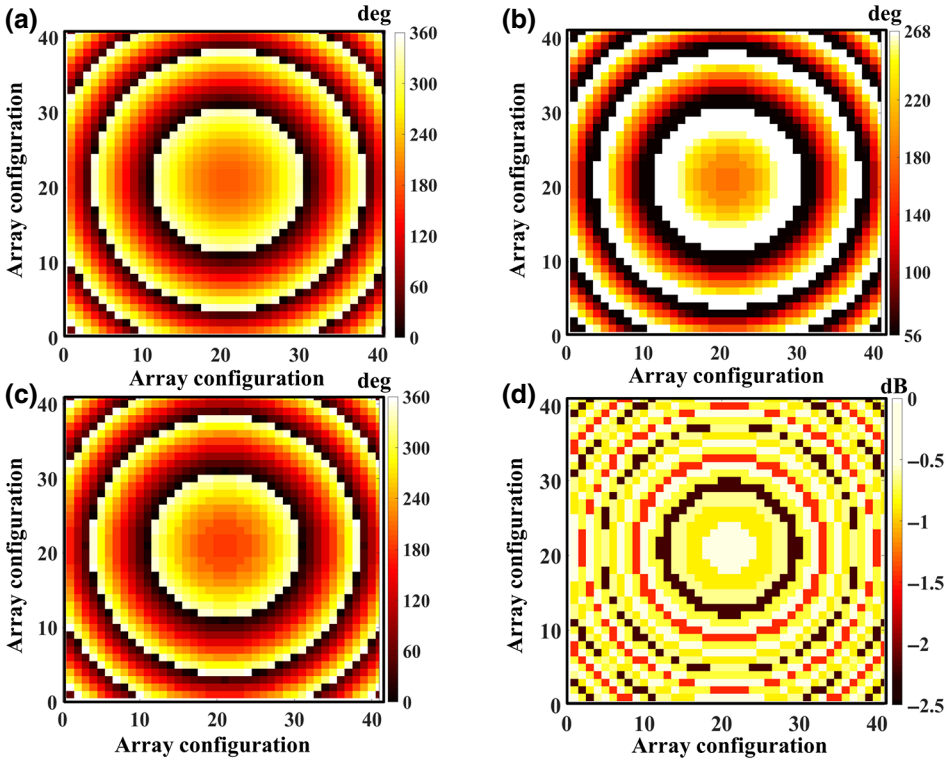

FIG. 7. The transmission phase and amplitude distributions of the double-layer transmitarray antenna at 13 GHz. (a) The required transmission phase distribution for the transmitarray design theoretically calculated by Eq. (3). (b) The realizable transmission phase distribution of the transmitarray composed of a symmetric unit structure. (c) The realizable transmission phase distribution of the transmitarray composed of an antisymmetric unit structure. (d) The realizable amplitude distribution of the transmitarray composed of antisymmetric unit structure.

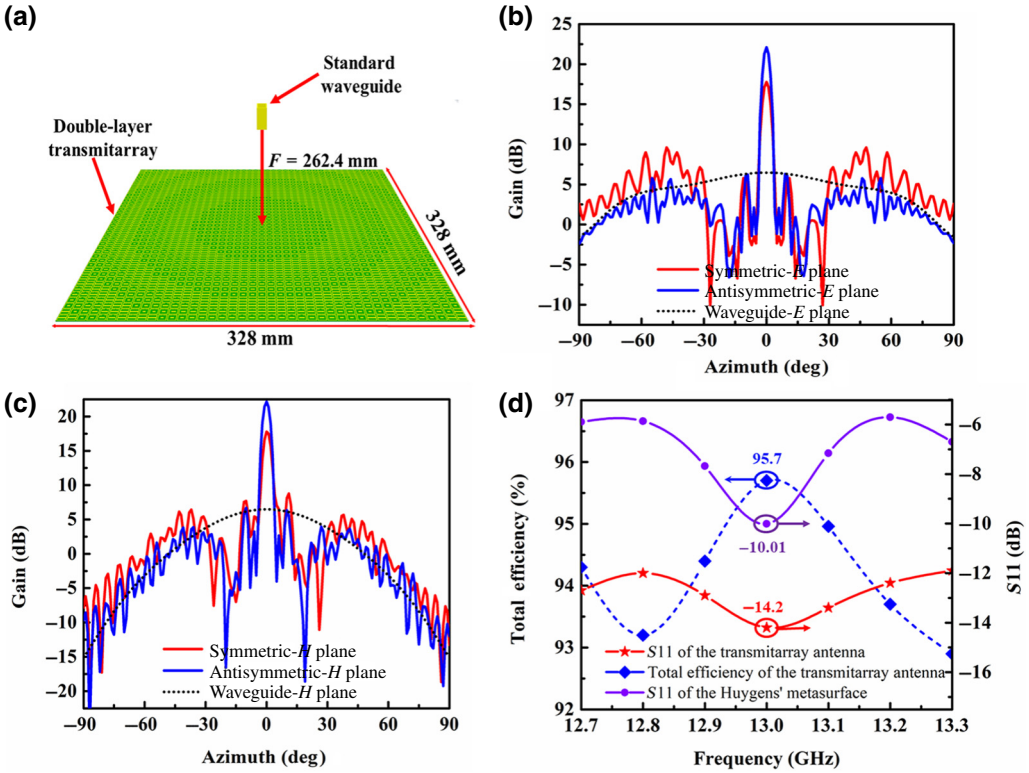

FIG. 8. The simulation setup and the simulated results of the double-layer transmitarray antennas fed by a standard waveguide. (a) The simulation setup. (b) The far-field radiation patterns of the E plane at 13 GHz. (c) The far-field radiation patterns of the H plane at 13 GHz. (d) The reflection coefficients of $S11$ for the transmitarray antenna and Huygens' metasurface, and the total efficiency of the transmitarray antenna.

(Z_{MS}/η) can also be calculated by Eqs. (1) and (2). According to the simulated transmission and reflection coefficients of different unit structures, the calculated $Y_{ES}\eta$ and Z_{MS}/η of points $P1$, $P2$, $P5$, and $P6$ at 13 GHz are listed in Table 1. The real parts of both normalized electric surface admittances and magnetic surface impedances at all points are almost equal and are very small, tending to zero, which implies the low loss of the unit structures. The imaginary parts are very different at points $P1$ and $P2$, corresponding to the large reflection and are very close at the points $P5$ and $P6$, corresponding to the high transmission, which are consistent with the conclusion that the Huygens' metasurface will be reflectionless when $Y_{ES}\eta = Z_{MS}/\eta$.

According to above discussion, the proposed double-layer antisymmetric unit structure can simultaneously achieve high transmissions and full 360° phase controls. Therefore, an ultrathin Huygens' metasurface can be constructed by using the proposed unit structure for arbitrary manipulations of wavefronts passing through the metasurface. A summarization of the unit structures that can cover a 360° phase shift with high transmission is listed in Table 2, which can be used for the design of ultrathin Huygens' metasurfaces with different functionalities.

III. DESIGN OF ULTRATHIN TRANSMITARRAY ANTENNA

Based on the proposed Huygens' metasurface, an ultrathin transmitarray antenna is designed, fabricated, and measured in this section. The sketch of the proposed transmitarray antenna is illustrated in Fig. 6. A feeding source is placed right above the transmitarray, and the distance between the source and transmitarray is F. In order to tailor the spherical incident waves into plane waves, the transmission phase of each element of transmitarray can be calculated by [18]

$$\varphi_i = k_0(R_{i\text{th}} - F) + \varphi_0, \tag{3}$$

where φ_i is the calculated phase of the ith element, φ_0 is the initial phase of the center element, $R_{i\text{th}}$ is the distance between the source and the ith element, and k_0 is the wave number in free space. Once the transmission phase of each element is achieved from Eq. (3), the corresponding unit cell can be chosen from Table 2 to construct the final transmitarray.

A double-layer transmitarray composed of 41×41 array elements is designed whose dimensions are 328×328 mm^2, and a feeding source is placed away from the transmitarray with a distance of $F = 262.4$ mm. In order to manipulate the spherical incident waves into plane waves, the transmission phase distribution of the transmitarray can be theoretically calculated according to Eq. (3), as illustrated in Fig. 7(a), which requires a full 360° phase shift. Traditionally, by using the symmetric unit structures shown in Fig. 2(b), the realizable transmission phase distribution of the transmitarray can only be designed to vary from 56° to 268° as shown in Fig. 7(b), which is due to the transmission phase control limitation of

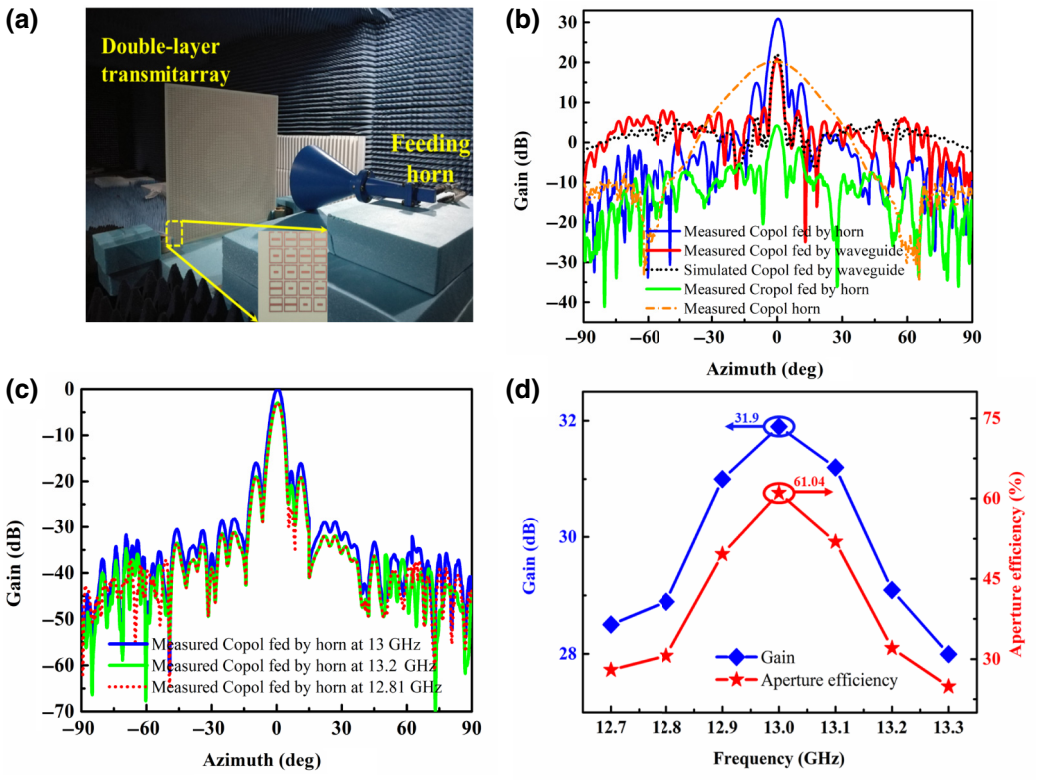

FIG. 9. The experimental setup and the measured results. (a) The experimental setup, fed by a corrugated horn. (b) Far-field radiation patterns of the E plane at 13 GHz. (c) The far-field radiation patterns at different frequencies. (d) Gains and aperture efficiencies varying with frequency of the proposed double-layer transmitarray antenna fed by a corrugated horn.

212° as demonstrated in Fig. 3(b). However, when the proposed antisymmetric unit structures are used to construct the transmitarray, the requirement of a full 360° transmission phase shift can be achieved as illustrated in Fig. 7(c), and the transmission amplitudes of elements are all larger than −2.5 dB as shown in Fig. 7(d).

The transmitarrays composed of both symmetric and antisymmetric unit structures are designed and simulated, respectively, based on the CST Microwave Studio®, as shown in Fig. 8. For convenience, a Ku-band standard waveguide is placed behind the transmitarrays as a feeding source, as demonstrated in Fig. 8(a). The simulated far-field radiation patterns of E and H planes at 13 GHz are shown in Figs. 8(b) and 8(c), respectively. The gain of the transmitarray antenna composed of antisymmetric unit structures is 22.5 dB, which is 4.5 dB higher than the transmitarray antenna composed of symmetric unit structures and 16 dB higher than the feeding source of the Ku-band standard waveguide. Figure 8(d) shows the simulated $S11$ and total efficiency of the designed antenna, which show that the $S11$ is less than −11.8 dB and the total efficiency is larger than 93% from 12.7 GHz to 13.3 GHz in which the total efficiency is defined as the ratio of radiation to input power of the antenna. In addition, we also further calculate the reflection coefficient ($S11$) of the designed Huygens' metasurface by full-wave simulation using CST®, as shown in Fig. 8(d) with the purple solid line, which shows that the $S11$ is less than −10.01 dB at 13 GHz. It is worth mentioning that the perfect electrical conductor (PEC) and perfect magnetic conductor (PMC) boundary conditions and wave ports are used in simulation to calculate the $S11$ of Huygens' metasurface. Hence, the conclusion can be made that quasispherical em waves generated by the feeding source can be efficiently converted to high-directivity plane waves by passing through the designed transmitarrays. However, the transmitarray antenna composed of an antisymmetric unit structures can achieve a better performance because of the precise 360° phase control.

The corrugated horn has a symmetric far-field radiation pattern and low cross-polarized level, which has been widely used in the measurement of transmitarray antennas as a feeding source [18,23,37]. In order to make a comparison with the published works in performance, the transmitarray antenna is remeasured by replacing the Ku-band standard waveguide with a corrugated horn as demonstrated in Fig. 9(a), and the measured far-field radiation pattern is also shown in Fig. 9(b) with the blue solid line. The measured gain is 31.9 dB, which is 10.1 dB higher than the transmitarray fed by the Ku-band standard waveguide and 11.5 dB higher than that of the corrugated horn. The side lobes are lower than −16 dB and the 3-dB gain bandwidth is 0.39 GHz (3%). The high cross-polarization level also can be observed from the measurement results, which is lower than −30.6 dB in the main beam direction. Since the generated wave of the Ku-band corrugated horn has similar E plane and H plane patterns [18], the H plane pattern of the transmistarray antenna, which is

TABLE III. The comparison of performances between the proposed transmitarray antenna and that of other publications.

Ref.	Working Freq. (GHz)	Number of layers	Thickness (λ)	Phase Range (°)	Gain (dB)	ϵ_{ap}
[39]	13.58	4	0.75	360	23.9	55%
[37]	13.5	4	0.765	360	30.22	50%
[38]	11.3	3	0.5	270	28.9	30%
[23]	20	2	0.104	305	33.0	40%
This work	13	2	0.033	360	31.9	61.04%

not provided, is nearly the same as those of the E plane patterns.

Compared to the Ku-band standard waveguide, the corrugated horn can focus the beam into a smaller region to aviod the diffraction of em waves, and the radiation pattern of emitting waves is almost circularly symmetrical, which can better satisfy the circular symmetry design of the transmission phases of the transmitarray. This is why the gain of the transmitarray antenna using the corrugated horn as a feeding source is about 10 dB higher than that using the Ku-band standard waveguide. Fig. 9(c) illustrates the far-field radiation patterns of the E plane at different frequencies, which show that the gain drops −3 dB as the frequency deviates about 0.2 GHz from the working frequency of 13 GHz. The reason for the quick drop of gain is the narrow bandwidth of the unit structures caused by the strong elecric and magnetic resonances, which also can be seen in the amplitude and phase responses shown in Fig. 5. Figure 9(d) shows the measured gains varying with the frequency of the proposed transmitarray antenna fed by the corrugated horn. The maximum gain of 31.9 dB is achieved at 13 GHz, but gradually decreases as the frequency deviates from 13 GHz.

According to the theory of antennas, the aperture efficiency (ϵ_{ap}) can be calculated by [38]

$$\varepsilon_{ap} = \frac{G}{D_{max}}, \tag{4}$$

where G is the measured gain, $D_{max} = 4\pi A_p/\lambda^2$ is the maximum directivity in which A_p is the physical aperture of the antenna, and λ is the wavelength at the working frequency. The gain of the proposed transmitarray antenna fed by the corrugated horn has been measured as 31.9 dB at 13 GHz, and the physical aperture of the transmitarray is 328×328 mm^2. Therefore, according to Eq. (4), the aperture efficiency of the transmitarray antenna can be achieved as illustrated in Fig. 9(d), which is up to 61.04% at 13 GHz.

Table 3 shows a comparison of the performances between the proposed transmitarray antenna and that of other publications. Because the proposed Huygens' metasurface has only two layers, the thickness of the transmitarray in this work is very thin, which is only 0.762 mm (0.033λ at 13 GHz). In addition, because the proposed Huygens' metasurface can simultaneously satisfy the high transmission and full 360° phase control, and the aperture efficiency of the transmitarray antenna in this work is much better than that is other published works.

IV. CONCLUSION

A simple method is presented to realize a high-transmission ultrathin Huygens' metasurface with a 360° phase control by only using double-layer transmitarray elements without vias. Different from the traditional symmetric unit structures, the two-layer antisymmetric structure can simultaneously introduce both electric and magnetic dipole resonances. Then high transmission and full 360° phase control can be achieved, which breaks the limitation of three layers using traditional technologies. Based on the proposed double-layer Huygens' structure, an ultrathin transmitarray antenna is designed, fabricated, and measured. The thickness of the transmitarray is only 0.033λ, while the measured gain can reach up to 61.04%, which has the advantages of ultrathin thickness and high gain over the published transmitarrays.

ACKNOWLEDGMENTS

This work was supported by the National Key Research and Development Program of China (Grants No. 2017YFA0700200, No, 2017YFA0700201, and No. 2017YFA0700202), the National Natural Science Foundation of China (Grants No. 61831006, No. 61571117, No. 61501117, No. 61501112, and No. 61631007), and the 111 Project (111-2-05).

[1] V. G. Veselago, The electrodynamics of substances with simultaneously negative values of ε and μ, Sov, Phys. Usp. **10**, 509 (1968).

[2] J. B. Pendry, A. J. Holden, W. J. Stewart, and I. Youngs, Extremely Low Frequency Plasmons in Metallic Mesostructures, Phys. Rev. Lett. **76**, 4773 (1996).

[3] T. J. Cui, D. R. Smith, and R. P. Liu, *Metamaterials: theory, design, and applications* (Springer Science & Business Media, New York, 2009).

[4] S. Zhang, W. Fan, N. C. Panoiu, K. J. Malloy, R. M. Osgood, and S. R. Brueck, Experimental Demonstration of Near-Infrared Negative-Index Metamaterials, Phys. Rev. Lett. **95**, 137404 (2005).

[5] R. Liu, C. Ji, J. J. Mock, J. Y. Chin, T. J. Cui, and D. R. Smith, Broadband ground-plane cloak, Science **323**, 366 (2009).

[6] H. F. Ma and T. J. Cui, Three-dimensional broadband ground-plane cloak made of metamaterials, Nat. Comm. **1**, 21 (2009).

[7] H. F. Ma and T. J. Cui, Three-dimensional broadband and broad-angle transformation-optics lens, Nat. Comm. **1**, 124 (2010).

[8] W. X. Jiang, H. F. Ma, Q. Cheng, and T. J. Cui, Illusion media: generating virtual objects using realizable metamaterials, Appl. Phys. Lett. **96**, 121910 (2010).

[9] N. F. Yu, P. Genevet, M. A. Kats, F. Aieta, J. P. Tetience, F. Capasso, and Z. Gaburro, Light propagation with phase discontinuities: generalized laws of reflection and refraction, Science **334**, 333 (2011).

[10] C. L. Holloway, E. F. Kuester, J. A. Gordon, J. O'Hara, J. Booth, and D. R. Smith, An overview of the theory and applications of metasurfaces: the two-dimensional equivalents of metamaterials, IEEE Antenn. Propag. Mag. **54**, 10 (2012).

[11] L. Zhang, S. T. Mei, K. Huang, and C. W. Qiu, Advances in full control of electromagnetic waves with metasurfaces, Adv. Opt. Mater. **4**, 818 (2016).

[12] S. B. Glybovski, S. A. Tretyakov, P. A. Belov, Y. S. Kivshar, and C. R. Simovski, Metasurfaces: from microwaves to visible, Phys. Rep. **634**, 1 (2016).

[13] Y. F. Yu, A. Y. Zhu, R. P. Dominguez, Y. H. Fu, B. Luk'yanchuk, and A. I. Kuznetsov, High-transmission dielectric metasurface with 360° phase control at visible wavelengths, Laser Photon. Rev. **9**, 412 (2015).

[14] X. Chen, Y. Zhang, L. Huang, and S. Zhang, Ultrathin metasurface laser beam shaper, Adv. Opt. Mater. **2**, 978 (2015).

[15] F. Qin, L. Ding, L. Zhang, F. Monticone, C. C. Chum, J. Deng, S. T. Mei, Y. Li, J. H. Teng, M. H. Hong, S. Zhang, A. Alu, and C. W. Qiu, Hybrid bilayer plasmonic metasurface efficiently manipulates visible light, Sci. Adv. **2**, e1501168 (2016).

[16] C. Pfeiffer and A. Grbic, Cascaded metasurfaces for complete phase and polarization control, Appl. Phys. Lett. **102**, 1232009 (2013).

[17] H. F. Ma, G. Z. Wang, G. S. Kong, and T. J. Cui, Broadband circular and linear polarization conversions realized by thin birefringent reflective metasurfaces, Opt. Mater. Express **4**, 1717 (2014).

[18] R. Y. Wu, Y. B. Li, W. Wu, C. B. Shi, and T. J. Cui, High-gain dual-band transmitarray, IEEE Trans. Antennas Propag. **65**, 3481 (2017).

[19] R. Y. Wu, C. B. Shi, S. Liu, W. Wu, and T. J. Cui, Addition theorem for digital coding metamaterials, Adv. Opt. Mater. **6**, 1701236 (2018).

[20] E. Erdil, K. Topalli, N. S. Esmaeilzad, Ö Zorlu, H. Kulah, and O. Civi, A Reconfigurable nested ring-split ring transmitarray unit cell employing the element rotation method by microfluidics, IEEE Trans. Antennas Propag. **63**, 1163 (2015).

[21] A. H. Abdelrahman, A. Z. Elsherbeni, and F. Yang, Transmission phase limit of multi-layer frequency selective surfaces for transmitarray designs, IEEE Trans. Antennas Propag. **62**, 690 (2014).

[22] M. Euler and V. F. Fusco, Frequency selective surface using nested split ring slot elements as a lens with mechanically reconfigurable beam steering capability, IEEE Trans. Antennas Propag. **58**, 3417 (2010).

[23] W. X. An, S. H. Xu, F. Yang, and M. K. Li, A double-layer transmitarray antenna using malta crosses with vias, IEEE Trans. Antennas Propag. **64**, 1120 (2016).

[24] C. Pfeiffer and A. Grbic, Metamaterial Huygens' Surfaces: Tailoring Wave Fronts with Reflectionless Sheets, Phys. Rev. Lett. **110**, 197401 (2013).

[25] C. Pfeiffer, N. K. Emani, A. M. Shaltout, A. Boltasseva, V. M. Shalaev, and A. Grbic, Efficient light bending with isotropic metamaterial Huygens' surfaces, Nano Lett. **14**, 2491 (2014).

[26] X. Wan, S. L. Jia, T. J. Cui, and Y. J. Zhao, Independent modulations of the transmission amplitudes and phases by using Huygens metasurfaces, Sci. Rep. **6**, 25639 (2016).

[27] S. L. Jia, X. Wan, D. Bao, Y. J. Zhao, and T. J. Cui, Independent controls of orthogonally polarized transmitted waves using a Huygens metasurface, Laser Photon. Rev. **9**, 545 (2015).

[28] M. Selvanayagam and G. V. Eleftheriades, Polarization control using tensor Huygens surfaces, IEEE Trans. Antennas Propag. **62**, 6155 (2014).

[29] X. Wan, L. Zhang, S. L. Jia, J. Y. Yin, and T. J. Cui, Horn antenna with reconfigurable beam refraction and polarization based on anisotropic Huygens metasurface, IEEE Trans. Antennas Propag. **65**, 4427 (2017).

[30] A. Mehdipour, J. W. Wong, and G. V. Eleftheriades, Beam-squinting reduction of leaky-wave antennas using Huygens metasurfaces, IEEE Trans. Antennas Propag. **63**, 978 (2015).

[31] J. P. S. Wong, M. Selvanayagam, and G. V. Eleftheriades, Design of unit cells and demonstration of methods for synthesizing Huygens metasurfaces, Photonics Nanostruct. **12**, 360 (2014).

[32] J. P. S. Wong, M. Selvanayagam, and G. V. Eleftheriades, Polarization considerations for scalar Huygens' metasurfaces and characterization for 2-D refraction, IEEE Trans. Microw. Theory Techn. **63**, 913 (2015).

[33] Michael Chen, Minseok Kim, Alex M. H. Wong, and George V. Eleftheriades, Huygens' metasurfaces from microwaves to optics: a review, Nanophotonics **7**, 1207 (2018).

[34] A. Epstein, J. P. S. Wong, and G. V. Eleftheriades, Cavity excited Huygens metasurface antennas for near-unity aperture illumination efficiency from arbitrarily large apertures, Nat. Commun. **7**, 10360 (2016).

[35] M. Chen, A. Epstein, and G. V. Eleftheriades, A Huygens' metasurface lens for enhancing the gain of frequency-scanned slotted waveguide antennas, USNC-URSI NRSM. Proceedings (2018) P1–2.

[36] F. Yang, R. Deng, S. Xu, and M. Li, Design and experiment of a near-zero-thickness high-gain transmit-reflect-array antenna using anisotropic metasurface, IEEE Trans. Antennas Propag. **66**, 2853 (2018).

[37] A. H. Abdelrahman, P. Nayeri, A. Z. Elsherbeni, and F. Yang, Bandwidth improvement methods of transmitarray antennas, IEEE Trans. Antennas Propag. **63**, 2946 (2015).

[38] A. H. Abdelrahman, A. Z. Elsherbeni, and F. Yang, High-gain and broadband transmit-array antenna using triple-layer spiral dipole elements, IEEE Antennas Wireless Propag. Lett. **13**, 1288 (2014).

[39] G. Liu, H. J. Wang, J. S. Jiang, F. Xue, and M. Yi, A high-efficiency transmitarray antenna using double split ring slot elements, IEEE Antennas Wireless Propag. Lett. **14**, 1415 (2015).